



## Abstract

A coarse grained, statically crystallized quartz vein, embedded in a phyllonitic matrix, was studied by EBSD and optical microscopy to gain insights into the processes of strain localization in quartz deformed under low-grade conditions, broadly coincident with the frictional–viscous transition. The vein is from a high strain zone at the front of the Porsa Imbricate Stack in the Paleoproterozoic Repparfjord Tectonic Window in northern Norway. The vein was deformed under lower greenschist facies conditions during deformation along a large out-of-sequence phyllonitic thrust of Caledonian age. The host phyllonite formed at the expense of metabasalt wherein feldspar broke down to form interconnected layers of fine, synkinematic phyllosilicates. In the mechanically weak framework of the phyllonite, the studied quartz vein acted as a relatively rigid body deforming mainly by coaxial strain. Viscous deformation was initially accommodated by basal  $\langle a \rangle$  slip of quartz during the development of a mesoscopic pervasive extensional crenulation cleavage. Under the prevailing boundary conditions, however, dislocation glide-accommodated deformation of quartz resulted inefficient and led to dislocation tangling and strain hardening of the vein. In response to hardening, to the progressive increase of fluid pressure and the increasing competence contrast between the vein and the weak foliated host phyllonite, quartz crystals began to deform frictionally along specific, optimally oriented lattice planes, creating microgouges along microfractures. These were, however, rapidly sealed by nucleation of new grains as transiently over pressured fluids penetrated the deforming system. The new nucleated grains grew initially by solution-precipitation and later by grain boundary migration. Due to the random initial orientation of the vein crystals, strain was accommodated differently in the individual crystals, leading to the development of remarkably different microstructures. Crystals oriented optimally for basal slip accommodated strain mainly viscously and experienced only minor fracturing. Instead, the crystals misoriented for basal slip hardened and deformed by pervasive domainal fracturing. This study indicates the importance of considering shear zones as dynamic systems wherein the ac-

SED

7, 213–257, 2015

### Brittle-viscous deformation of vein quartz

H. J. Kjølil et al.

Title Page

Abstract

Introduction

Conclusions

References

Tables

Figures

◀

▶

◀

▶

Back

Close

Full Screen / Esc

Printer-friendly Version

Interactive Discussion



tivated deformation mechanisms vary transiently in response to the complex temporal and spatial evolution of the shear zone, often in a cyclic fashion.

## 1 Introduction

Deformation of quartz at low-grade metamorphic conditions has been the subject of a vast number of microstructural studies aiming to unravel the mechanisms that control strain accommodation therein and to derive parameters of general validity for the rheology of quartz-rich systems at shallow to mid crustal levels (e.g. Trepmann and Stöckhert, 2009; Stipp et al., 2002; Menegon et al., 2008; Holyoke and Tullis, 2006; Dell'Angelo and Tullis, 1996; Hirth and Tullis, 1992; Stipp and Kunze, 2008). In spite of significant recent advances, however, much remains unexplored and unaccounted for, such as the role of fluid-rock interaction on the microstructural development of quartz, the effect of contrasting rheology and of the resulting strain partitioning between matrix and quartz porphyroclasts, and the relationship between the orientation of newly formed crystals and the dominant stress field. Recent technological developments have made powerful methodologies such as electron backscattered diffraction (EBSD; e.g. Adams et al., 1993; Prior et al., 1999, 2009) readily available. This permits extremely detailed investigations and quantification of microstructures and thereby, the derivation of highly refined conceptual models of the deformation mechanisms in quartz at the broadly defined frictional–viscous transition.

The occurrence of complex intragrain quartz microstructures characterized by bands of new grains in large porphyroclasts has been noted and described as standard for low-grade deformed quartz in a number of studies (e.g. Vernooij et al., 2006b; van Daalen et al., 1999; Menegon et al., 2008). These microstructures tend to develop during the very early stages of viscous deformation of quartz and are thus believed to be the key to understand strain localization under very low-grade metamorphic conditions. Three mechanisms have been proposed to explain their occurrence: (1) progressive sub grain rotation recrystallization (Bestmann and Prior, 2003), (2) intrapore growth by

SED

7, 213–257, 2015

### Brittle-viscous deformation of vein quartz

H. J. Kjøll et al.

Title Page

Abstract

Introduction

Conclusions

References

Tables

Figures

⏪

⏩

◀

▶

Back

Close

Full Screen / Esc

Printer-friendly Version

Interactive Discussion



dissolution-precipitation (e.g. den Brok and Spiers, 1991; Hippertt and Egydio-Silva, 1996) and (3) fracturing along specific crystallographic planes with subsequent fragment rotation (e.g. den Brok, 1992; van Daalen et al., 1999; Vernooij et al., 2006b). Van Daalen et al. (1999) investigated the importance of crystallographic orientation with respect to the stress field as they observed that bands of new grains tend to develop along the rhomb direction within the deforming crystal. Trepmann et al. (2007) studied further the importance of these microstructures by means of carefully designed experiments, wherein they investigated deformation at the tip of a seismic fault. They could reproduce similar microstructures by deforming quartz under high stresses before annealing it under quasi-static conditions.

We aim herein to investigate further how these characteristic microstructures develop in quartz at the frictional–viscous transition in a tectonically active environment wherein fluids and competence contrasts between the actively deforming mineral phases induce cyclic oscillations between frictional and viscous conditions. To do so, we studied in detail the microstructure of a quartz vein embedded in a phyllonitic matrix. The vein, which crystallized statically prior to deformation, permits an assessment of the influence exerted by the random initial orientation of the deformed crystals on the accommodation of subsequent strain increments by either frictional or viscous processes. The lack of an initial CPO caused the development of drastically different end microstructures within a very small volume of rock, thus allowing the critical and comparative analysis of the many different deformation mechanisms that acted simultaneously during deformation.

Furthermore, our observations help to better evaluate the role played by the rheological contrast between the vein and the mechanically weaker phyllonitic host rock.

## SED

7, 213–257, 2015

### Brittle-viscous deformation of vein quartz

H. J. Kjølil et al.

Title Page

Abstract

Introduction

Conclusions

References

Tables

Figures



Back

Close

Full Screen / Esc

Printer-friendly Version

Interactive Discussion



## 2 Geological setting

### 2.1 Regional geological setting and structural framework

This microstructural study was carried out as part of a larger structural project dealing with the mapping, characterization and dating of a major imbricate structure. The study area is located within the Repparfjord Tectonic Window (RTW), the northernmost exposed termination of the Fennoscandian Shield in northern Norway (Fig. 1). The RTW is a window through the Kalak Nappe Complex of the upper allochthon of the Scandinavian Caledonides, which consists of greenschist to amphibolite-facies metapelites, metapsammites and marbles, with intercalated gneissic slivers (e.g. Gee et al., 2008; Roberts, 2003; Torgersen et al., 2014). The RTW exposes a package of metasedimentary and metavolcanic rocks, ranging from the clastic and volcanoclastic rocks of the Saltvann Group to the ultramafic to rhyolitic calc-alkaline to tholeiitic volcanites of the Holmvann and Nussir Groups (Pharaoh, 1985; Pharaoh et al., 1983). The Porsa Group at the top is formed by stromatolitic dolostones and slates with varying graphite and carbonate content. These lithologies are supposedly of Paleoproterozoic age based on correlations with other Paleoproterozoic belts of the Fennoscandian Shield (Pharaoh et al., 1983). K–Ar dating suggests that they deformed under greenschist-facies conditions until ca. 1840 Ma ago, with formation of km-scale upright folds (e.g. Pharaoh et al., 1982).

The northwestern most part of the RTW is formed by a set of strongly deformed tectonic imbricates, stacked up to form the Porsa Imbricate Stack (PIS; Torgersen and Viola, 2014; Fig. 1a). Shortening and imbrication within the PIS occurred during the Silurian-aged Caledonian orogeny, which emplaced the Kalak Nappe Complex (KNC) onto the westernmost edge of the Fennoscandian Shield during overall NW–SE shortening and ca. E-ward transport direction (Rice, 1998). As deformation started to localize during development of the PIS, discrete thrust faults nucleated on the limbs of inherited Paleoproterozoic folds. These tightened and acquired a SE-vergence during

## Brittle-viscous deformation of vein quartz

H. J. Kjølil et al.

Title Page

Abstract

Introduction

Conclusions

References

Tables

Figures



Back

Close

Full Screen / Esc

Printer-friendly Version

Interactive Discussion







crystallographic preferred orientation (CPO) of the vein quartz by EBSD analysis at the SEM. To enhance the diffraction signal, thin sections were polished using colloidal silica for 5 min (Moen et al., 2003) and placed in a Hitachi VP-SEM with a Nordiff fast acquisition UF-1000 EBSD detector (Chen et al., 2012) at a 70° tilt to the electron beam (Prior et al., 1999). To acquire a satisfactory pattern quality the accelerating voltage used was 20.0 kV at 35 nA absorbed current. The working distance was set to 25.3 mm and the step size to 2 µm. The data was processed using the open source Matlab toolbox MTEX 3.5.0 (e.g. Bachmann et al., 2010; Mainprice et al., 2011). Further analysis of the EBSD data was conducted using NIH image (Schneider et al., 2012).

## 4 Results

### 4.1 Sample description

The studied sample is from a quartz vein and its host rock within the ramp of the NFZ (green star in Figs. 1 and 2), where the main foliation developed at the expense of the Nussir metabasalts. The vein is cut and offset by top-to-the SE shear bands that impart the outcrop a pervasive ECC. The hand specimen is a well-foliated phyllonitic rock containing a centimetric clast of the quartz vein bound by- and offset along one centimetric shear band, with numerous smaller shear bands also deforming the vein (Fig. 3). The phyllonitic foliation is passively dragged into the shear bands confirming the kinematics determined by field observations (Figs. 2a, 3a and 4a).

The phyllonitic foliation is defined by bands consisting of varying amounts of feldspathic clasts with albitic composition within a phyllonitic matrix of sericitic white mica and chlorite. The grain size of the phyllonite is very fine, usually < 50 µm, except for some residual dolomitic porphyroclasts, which are up to > 1 mm in size. Feldspar clasts range in size from < 100 to > 500 µm. They can be locally asymmetrically boudinaged and deformed by small shear bands and exhibit partial recrystallization localized in the

SED

7, 213–257, 2015

## Brittle-viscous deformation of vein quartz

H. J. Kjøl et al.

Title Page

Abstract

Introduction

Conclusions

References

Tables

Figures

⏪

⏩

◀

▶

Back

Close

Full Screen / Esc

Printer-friendly Version

Interactive Discussion



neck zones of the boudins (Fig. 4a). The small-scale shear bands locally indicate both dextral and sinistral sense of shear, suggesting a component of flattening.

Several euhedral sulfide porphyroblasts, partially broken down to oxides, are dispersed in the phyllonite and within the vein; some are also symmetrically boudinaged and show fibrous quartz growth in the neck domains and pressure shadows (Fig. 4b). Sigmoidal dolomite porphyroclasts are commonly observed. Syntaxially-filled calcite veinlets are observed sub-parallel to the mylonitic foliation. These veinlets accommodated more than one opening event (Fig. 4e).

The studied vein clast consists primarily of quartz with pockets of primary calcite. Minor secondary calcite and accessory sulfides are found both within the quartz crystals and along the grain boundaries. Quartz crystals within the vein range in size from  $< 0.5$  to  $> 6$  mm, do not show a crystal preferred orientation (CPO; Figs. 6–9b) and no shape preferred orientation (SPO). In general, the boundaries between the individual grains are slightly irregular but straight, which gives the individual quartz crystals a blocky appearance. Calcite filled intra-vein fractures indicate localized post vein deformation.

## 4.2 Microstructural and EBSD analysis

Because of the marked textural differences that we have observed within the quartz vein, we have identified and studied in detail distinct microstructural domains, each characterized by internally consistent microstructures. Our study reports four representative domains that are described individually below. Table 1 and Figs. 6–9 sum up the main CPO elements constrained by petrographic and EBSD analysis.

Several quartz crystals contain narrow bands of much finer grains. In the text these grains are referred to as “new grains” and are distinguished from the parent grains or “old grains” based on aspect ratio, grain size and primarily on their misorientation angle to neighbor grains. In detail, all grain boundaries were defined as misorientations larger than  $10^\circ$ .

SED

7, 213–257, 2015

## Brittle-viscous deformation of vein quartz

H. J. Kjøll et al.

Title Page

Abstract

Introduction

Conclusions

References

Tables

Figures

⏪

⏩

◀

▶

Back

Close

Full Screen / Esc

Printer-friendly Version

Interactive Discussion



## 4.2.1 Domain 1

*Domain 1* (Fig. 3b and c) is found within a single crystal measuring  $6 \times 3$  mm. It contains a tightly spaced set of sub-parallel and semi-straight bands of nucleated grains. The grains vary in size between ca. 10 and  $60 \mu\text{m}$ , have a slightly elongated shape and constitute ca. 40% of the area of the domain. The bands are continuous for several millimeters and are on average  $30 \mu\text{m}$  thick (1–3 grains thick). We name this microstructure “striped tiger”. Some bands also contain small (ca.  $50 \mu\text{m}$  in size) calcite grains interspersed among the new quartz grains. The bands are sub-parallel to the  $C'$  shear bands that offset the quartz vein. Bridges between the most pronounced bands are observed (white arrow in Fig. 3c).

The host grain displays undulose extinction, which is defined by wide extinction bands (WEB; Derez et al., 2014; Black dashed line in Fig. 3c). WEB's have an anti-thetic geometry to the large shear band that cuts through and offsets the quartz vein in the hand specimen (Fig. 3a) and are themselves cut by the bands of new grains (Fig. 3b and c).

EBSD analysis of the sub parallel bands of new grains shows that they range in size between ca. 5 and  $50 \mu\text{m}$  (Fig. 6f and Table 1), and have a different crystallographic orientation from the host (Fig. 6d). The  $c$  axis of the host grain in domain 1 is in the foliation plane at ca.  $20^\circ$  from the stretching lineation and is visualized by the orange color in Fig. 6a and b, while the red color represents Dauphiné twins, which accommodate a  $60^\circ$  rotation around the [0001] and are thus not visible under the optical microscope (Frondel et al., 1962). As noted above, there are two sets of bands in the domain, one pervasively developed and one subordinate. The more developed set contains bands that are sub-parallel to the prism plane of the host old grain (dashed line in right stereonet Fig. 6b) and thus are oriented sub-parallel to the sample-scale  $C'$  shear band and with an average  $23^\circ$  angle to the foliation, when measured counterclockwise. The less developed bands are seen in the lower left corner of the EBSD map (white arrow in Fig. 6a) and are sub-parallel to the rhomb (dashed line in middle

# SED

7, 213–257, 2015

## Brittle-viscous deformation of vein quartz

H. J. Kjøll et al.

Title Page

Abstract

Introduction

Conclusions

References

Tables

Figures

⏪

⏩

◀

▶

Back

Close

Full Screen / Esc

Printer-friendly Version

Interactive Discussion



stereonet Fig. 6b) forming an angle of  $138^\circ$  to the foliation, *S*, measured counterclockwise. The new grains within the bands are slightly elliptical with an average aspect ratio of 1.63 and average grain size of  $15.51 \mu\text{m}$  (Fig. 6e and f). The new grains have a more scattered *c* axis distribution (Fig. 6c), possibly reflecting a clockwise rotation around a sub-vertical axis causing their distribution to fade towards the periphery and the “north” of the pole figure. They display large misorientations (locally  $> 40^\circ$ ) to each other and to the host, There is no progressive rotation of the lattice when approaching the bands from the host, i.e. the change in misorientation is abrupt, thus excluding recovery and recrystallization by subgrain rotation (Fig. 6d).

#### 4.2.2 Domain 2

*Domain 2* is located at the tip of the quartz vein, where the latter is sandwiched by the foliation *S* and the micaceous shear plane *C'* of the host phyllonite (Fig. 3b). It contains abundant secondary calcite. Grain size distribution is unimodal, with equigranular and equidimensional grains. It is almost completely made up of nucleated new grains (Fig. 3d), although some local relics of a few host old grains (up to  $80 \mu\text{m}$  in size) can still be recognized (Fig. 7a).

*Domain 2* is pervasively recrystallized (Fig. 3d) with only small amounts of preserved old grains, as shown by the presence of local sub grain boundaries within the larger and more irregular crystals (Fig. 7a). The old grains form a *c* axis maximum around the N and S poles of the pole figure, with only a weak counterclockwise deflection (Fig. 7b). As far as the new grains are concerned, *Domain 2* has the largest average grain size of all domains and the highest average aspect ratio, with  $18.03$  and  $1.66 \mu\text{m}$ , respectively (Fig. 7e and f and Table 1). There is no obvious preferred elongation direction of the new grains (Fig. 7e). The new grain crystallographic orientations are scattered compared to the old grains. The new grains have a high and sharp misorientation to each other and to the old grains, locally close to  $90^\circ$ . No progressive lattice rotation is visible in the old grains towards the new grains (Fig. 7d).

### Brittle-viscous deformation of vein quartz

H. J. Kjølil et al.

Title Page

Abstract

Introduction

Conclusions

References

Tables

Figures



Back

Close

Full Screen / Esc

Printer-friendly Version

Interactive Discussion



### 4.2.3 Domain 3

The upper part of the vein hosts a large grain measuring  $5 \times 3$  mm, which hosts *Domain 3* of our study (Fig. 3b and e). The grain displays sweeping and patchy undulose extinction with upright WEBS and two sets of bands of new grains. The new grains in these bands are less developed than in other domains. The most pronounced set is recognized due to its slightly different extinction direction with regard to the host. Generally, there are few new grains within these bands, although some local, isolated pockets of new grains occur (Fig. 3e). The new grains are encircled by large fluid inclusions and some tiny muscovite grains (Fig. 4d), and their grain boundary microstructure show evidence for porosity and dissolution-precipitation features (e.g. Mancktelow and Pennacchioni, 2004; Fig. 5). The bands and fluid inclusion trails define patchy undulose extinction patterns (bLEB; Derez et al., 2014). The second set of bands is seen as semi-straight trails of fluid inclusions, with no visible recrystallization. The left half of the domain is characterized by sub-parallel fluid inclusion trails. No nucleation of new grains is seen along these traces (white arrows in Fig. 3e).

Only local bands and clusters of new grains are observed in *Domain 3*, which is the domain with the lowest density of new grains (Fig. 8a). The *c* axis of the host old grain is subparallel to the *Z* direction of finite strain, and slightly inclined with the bulk sinistral sense of shear (Fig. 8b). The host old grains display a clear single-crystal maximum with very little dispersion around both the  $\langle c \rangle$  and  $\langle a \rangle$  axis, although some undulose extinction can be inferred from the different shades of blue. The bands and clusters of new grains are oriented at  $20^\circ$  with respect to the foliation *S*, measured counterclockwise, which makes them sub-parallel to the basal plane of the old grain (dashed line in Fig. 8b). The bands often define high angle sub grain boundaries, close to true grain boundaries, within the host grain (black arrows in Fig. 8a and d). In the central and left parts of *Domain 3* fluid inclusion trails are observed. These trails are sub-parallel to the rhomb direction (white arrows in Figs. 3e and 8b) and are oriented at  $150^\circ$  measured counterclockwise from the foliation *S*.

SED

7, 213–257, 2015

## Brittle-viscous deformation of vein quartz

H. J. Kj  ll et al.

Title Page

Abstract

Introduction

Conclusions

References

Tables

Figures

⏪

⏩

◀

▶

Back

Close

Full Screen / Esc

Printer-friendly Version

Interactive Discussion



**Brittle-viscous  
deformation of vein  
quartz**

H. J. Kjøllet et al.

[Title Page](#)[Abstract](#)[Introduction](#)[Conclusions](#)[References](#)[Tables](#)[Figures](#)[Back](#)[Close](#)[Full Screen / Esc](#)[Printer-friendly Version](#)[Interactive Discussion](#)

The average grain size of the new grains is  $13.96\ \mu\text{m}$  (Fig. 8e and Table 1) and they have an average aspect ratio of 1.59 (Fig. 8f) with the preferred elongation at  $115^\circ$  measured counterclockwise from the foliation  $S$ . The crystallographic distribution of the new grains is more scattered than for the old grains (Fig. 8c and b, respectively).

The data seems to have been rotated clockwise around a sub-vertical rotation axis. This domain has the smallest grain size, both average and maximum and the lowest aspect ratio (Table 1 and Fig. 8e and f). The measured misorientation profile shows that the orientation difference between neighbor old grains is quite large. Locally sub grain boundaries represent misorientations in excess of the threshold value of  $10^\circ$  (black arrows in Fig. 8a and d), while new grains display misorientations  $> 20^\circ$  (Fig. 8d).

#### 4.2.4 Domain 4

*Domain 4* is a relatively small, single crystal measuring  $2 \times 0.5\ \text{mm}$  (Fig. 3b and f). Above the crystal there is a high density of feldspar clasts wrapped in an anastomosed phyllonitic matrix with shear indicators suggesting an opposite sense of shear to the top-to-the SE regional sense of shear accommodated by the NFZ. Microstructurally the crystal resembles *Domain 1*, with a “striped tiger” microstructure; in *Domain 4*, however, two well-developed sets of bands with new grains occur, in contrast to *Domain 1* where there is only one well-developed direction. One direction, inclined towards the right, is the most pronounced, while the one, inclined to the left, is slightly less pervasive in the crystal. The traces of the two bands are separated by ca.  $70^\circ$ . The lambda plate reveals that the main band of new grains also separates two sub domains within the single crystal with a slight misorientation with respect to each other. The crystal contains some randomly arranged fluid inclusions.

*Domain 4* has an old grain with a  $c$  axis located in an intermediate position between the  $Z$  and  $Y$  axis of strain and slightly inclined with the bulk sinistral sense of shear (Fig. 9a and b). Undulose extinction is seen as different shades of orange. Red represents Dauphiné twins. The two identified sets of bands are parallel to the prism and the rhomb, they form a  $50$  and  $120^\circ$  angle, respectively, measured counter clockwise from

the foliation *S* (dashed lines in the middle and right stereonet in Fig. 9b and Table 1). The average aspect ratio is 1.60 and the average grain size is 15.48  $\mu\text{m}$  and (Fig. 9e and f) with an elongation direction of  $104^\circ$  measured counterclockwise from the horizontal *S*. In addition, the new grains define a more scattered *c* axis distribution, with no clear directional trend (Fig. 9c). A misorientation profile along one of the rhomb bands shows that the recrystallized grains are rather strain free, with very little internal misorientation and often separated by quite high angles up to  $70^\circ$ . The boundary between the old grain and the recrystallized bands are sharp and not progressive (Fig. 9d).

## 5 Discussion

### 5.1 Strain accommodation history within the different domains

Our dataset documents examples of quartz microstructures developed in a fluid rich system deformed under low-grade metamorphic conditions. Initial embrittlement of the host greenstones was accommodated by fracturing, fluid circulation and quartz (and carbonate) precipitation as vein material. The crystallization of the vein occurred statically, resulting in a random crystallographic orientation of the constituting large quartz crystals. Pervasive viscous deformation led to the strain accommodation within the vein and the development of the ECC fabric in the host greenstones. Viscous deformation, however, was itself interrupted by transient episodes of embrittlement, which we relate to both the crystallographic framework inherited from the statically crystallized vein and the oscillations of the pressure of the fluid phase that was present during continued deformation related to the thrusting history along the NFZ.

This structural evolution is summarized conceptually in Fig. 10, is supported by the summary of Table 1 and is discussed in detail below.

Following initial fracturing and vein crystallization (possibly related to early Caledonian deformation or even to the Paleoproterozoic evolution of the region; Fig. 10a), the vein became progressively involved in the Caledonian deformational history of the NFZ,

SED

7, 213–257, 2015

## Brittle-viscous deformation of vein quartz

H. J. Kjølil et al.

Title Page

Abstract

Introduction

Conclusions

References

Tables

Figures

⏪

⏩

◀

▶

Back

Close

Full Screen / Esc

Printer-friendly Version

Interactive Discussion



wherein top-to-the SE thrusting led to the progressive development of the shear zone. Environmental conditions were such that quartz began to deform by low-grade crystal plastic deformation by dislocation glide (Fig. 10b). Two main mechanisms are believed to have controlled this stage of the system microstructural evolution: (1) strain partitioning resulting from the high competence contrast between the vein and the surrounding greenstone, which was evolving into a progressively foliated and finer-grained phyl-  
lonite as strain was accommodated in the core of the NFZ (Trepmann and Stöckhert, 2009), and (2) presence of fluids as documented by the numerous veinlets, secondary phases trapped along grain boundaries (Fig. 4d) and fluid inclusions (Fig. 5; e.g. Drury and Urai, 1990; Mancktelow and Pennacchioni, 2004; Fig. 10b). Low-grade viscous deformation produced structures such as bulging grain boundaries (Fig. 4c) caused by slow grain boundary migration (Stipp et al., 2002), sweeping undulatory extinction, bLEB, WEB (Derez et al., 2014; Fig. 3b–f) and drag folds (Fig. 10b). EBSD analysis has shown remarkably different microstructures and CPO patterns in the analyzed domains that can be assigned to this microstructural stage. We ascribe this to the fact that each domain had a different crystallographic orientation, due to the static initial crystallization in the vein.

*Domain 1*, for example, would have been optimally oriented for viscous slip to be accommodated along either the prism (*a*) or prism (*c*) (Fig. 6b). In order to be activated, however, these slip planes require higher-grade conditions than those at which the vein was deforming (Schmid and Casey, 1986; Stipp et al., 2002). Synkinematic chlorite thermometry from similar faults in the area has established a peak temperature of < 300 °C, ideal for activation of basal  $\langle a \rangle$  slip. The crystal was, however, misoriented for basal  $\langle a \rangle$  slip. Some strain was nonetheless taken up in a ductile fashion in *Domain 1* by the development of WEBs (Derez et al., 2014). Since easy-glide planes were oriented at a high angle to the *C'* shear band, dislocation glide resulted soon ineffective, leading in turn to dislocation tangling, strain hardening and localized embrittlement of the deforming quartz accommodated by diffuse fracturing. Transiently high fluid pressure is also believed to have contributed to localized and short-lived embrittlement as the fluid

## SED

7, 213–257, 2015

### Brittle-viscous deformation of vein quartz

H. J. Kjøll et al.

Title Page

Abstract

Introduction

Conclusions

References

Tables

Figures



Back

Close

Full Screen / Esc

Printer-friendly Version

Interactive Discussion



factor  $\lambda$  approached unit value (e.g. Cox, 2010; Hubbert and Rubey, 1959; Fig. 10c). Evidence for fluid-accompanied fracturing, such as fluid inclusion trails (Fig. 5b and c), is invariably found in the studied samples and within the NFZ in general (Fig. 10c).

The fractures developed during this stage of the structural evolution of *Domain 1* are invariably intra-granular, which points towards sub critical crack growth, by, for example, stress corrosion, microplasticity or general plasticity (e.g. Atkinson, 1982, 1984; Stünitz and Fitz Gerald, 1993). Development of volumetrically small gouges along the fracture planes is also envisaged (Fig. 10c1). The fracture sub-parallel orientation suggests in addition that they formed controlled by specific lattice planes, that is, planes with a low density of covalent bonds and thus low surface energy (Figs. 6, 8 and 9; e.g. Fairbairn, 1939; Flörke et al., 1981; Vollbrecht et al., 1999; van Daalen et al., 1999).

The weakest crystallographic plane in quartz is the rhomb. van Daalen et al. (1999) report what they refer to as “micro shear zones”, that is, bands of new grains, along the positive and negative rhomb planes. The two sets of bands with nucleated new grains within *Domain 1* are sub-parallel to the prism and the rhomb face of the crystal. The prism plane direction, parallel to which we find the most pervasive set of bands of new grains, was the optimally oriented direction for brittle failure, as it is sub-parallel to the actual slip plane of the mesoscopic system, that is, the shear band (Fig. 6e). The rhomb, although oriented at a high angle to the shear band, is the weakest crystallographic plane in quartz, and, therefore, it did also fail. The geometric orientation of the rhomb was such that it was suitably oriented to accommodate strain along the antithetic direction of a conjugate set of fractures. This suggests that a component of flattening characterized the NFZ deformation, as also indicated by numerous conjugate shear bands in the surrounding phyllonitic matrix.

In summary, the “striped tiger” microstructure observed within *Domain 1* is best interpreted in terms of “sealing” of these earlier micro-fractures by nucleation of new grains (Fig. 10d1). This mechanism is discussed in more detail in Sect. 6.2.

In contrast to *Domain 1*, *Domain 3* was suitably oriented for effective accommodation of viscous deformation, with the basal plane oriented sub-parallel to the  $C'$  shear band,

SED

7, 213–257, 2015

## Brittle-viscous deformation of vein quartz

H. J. Kjølil et al.

Title Page

Abstract

Introduction

Conclusions

References

Tables

Figures

⏪

⏩

◀

▶

Back

Close

Full Screen / Esc

Printer-friendly Version

Interactive Discussion



that is, optimally oriented for slip along the basal  $\langle a \rangle$  (Schmid and Casey, 1986). This is because the crystallographic orientation inherited from the primary static crystallization of the vein in *Domain 3* was already optimal for accommodating strain under viscous conditions. The pole figure of the old grains shows indeed a single crystal maximum in the location expected for quartz deformed under lower greenschist facies conditions (Stipp et al., 2002). *Domain 3*, however, also contains two sets of bands with new grains (Figs. 3e and 8). As in the case of *Domain 1*, we interpret these as sealed fractures, with one set oriented sub-parallel to the basal plane of the crystal and the second sub-parallel to the rhomb plane (Figs. 6b and 10c). The “striped tiger” microstructure, however, is much less pervasive than in *Domain 1*. We explain this by the less pervasive domainal fracturing that would have affected *Domain 3*. A crystal with the orientation of *Domain 3* would have been more prone to accommodate strain by dislocation glide and would not strain harden as much as that of *Domain 1*. In addition, one set of fractures would have had to form along the basal plane of the crystal, which is not a crystal face with particularly low surface energy. As for the second set, sub-parallel to the rhomb, EBSD analysis reveals that some new grains developed also along these fractures, but mostly in the junctions where the two fracture sets intersect. However, new grain nucleation along fracture planes parallel to the rhomb is not nearly as pervasive as the other fracture in the same domain or any of the other fractures in *Domain 1* (Figs. 8a and 6a). We suggest that these fractures opened during an earlier embrittlement event, possibly under different physical boundary conditions, wherein the fractures healed by epitaxial growth on the fracture wall.

The quartz crystal of *Domain 4* was oriented similarly to the one in *Domain 1* and it thus underwent only limited crystal-plastic deformation, with the latter strongly inhibited by early dislocation tangling resulting in undulose extinction and progressive strain hardening and domainal fracturing. Similarly to *Domain 1*, *Domain 4* is also characterized by the fracturing along the prism and the rhomb plane (Fig. 9b). Both directions are fairly well developed, but the prism-parallel bands are more continuous. In this domain the rhomb-parallel set is parallel to the  $C'$  shear band, while the prism-parallel

## SED

7, 213–257, 2015

### Brittle-viscous deformation of vein quartz

H. J. Kjøllet et al.

Title Page

Abstract

Introduction

Conclusions

References

Tables

Figures



Back

Close

Full Screen / Esc

Printer-friendly Version

Interactive Discussion





## Brittle-viscous deformation of vein quartz

H. J. Kjølil et al.

Title Page

Abstract

Introduction

Conclusions

References

Tables

Figures



Back

Close

Full Screen / Esc

Printer-friendly Version

Interactive Discussion



fluid (solution-precipitation; Vernooij et al., 2006a) or by solution transfer from one pore wall to another (dissolution-precipitation; Hippertt and Egydio-Silva, 1996). This model explains *Domain 1* and *4*, where fractures formed pervasively, with possible micro displacements even locally accommodated along individual fracture planes. These displacements were likely obliterated by later quartz dissolution at the grain boundaries. In *Domain 3*, where fracturing was minimal due to the favorable orientation of the crystal for basal  $\langle a \rangle$  dislocation glide, less energy was required to maintain steady state crystal-plastic deformation and significant embrittlement was not achieved; hence, no bands of new grains sealing older fractures were produced, and instead only local pockets of newly formed, strain free grains crystallized. These pockets and a few only poorly developed bands are all oriented along discrete sub grain- to grain boundaries with relatively high misorientations across ( $10 \pm 3^\circ$ ; Fig. 8a and d), which may have acted as conduits for fluids during deformation and initiated dissolution-precipitation in pores and solution-precipitation along micro fractures oriented along the sub grain- and grain boundaries. Fluid infiltration may also have led to hydrolytic weakening, which is known to promote local climb-accommodated dislocation creep (e.g. Kronenberg et al., 1990; Mancktelow and Pennacchioni, 2004). This could account for the few observed bands of subgrains. The growth of new grains within pores is well described by Hippertt and Egydio-Silva (1996) and results in intrapore grains, which first grow by dissolution-precipitation followed by grain boundary migration when they touch the opposite fracture wall (Fig. 10c1 and c2). As the new grains are largely strain free they grew at the expense of the old grains, which have a higher dislocation density (e.g. Drury and Urai, 1990). Furthermore, Schmid and Casey (1986) proposed that grains growing by grain boundary migration tend to grow optimally oriented for basal slip, i.e. with the basal plane at  $45^\circ$  to  $\sigma_1$  (Vernooij et al., 2006a). This mechanism could also contribute to the rotation of the new grain crystals seen in the EBSD data (Fig. 6).

As also proposed by several authors (e.g. Derez et al., 2014; Vernooij et al., 2006a; Trepmann et al., 2007), we conclude that dynamic recrystallization by sub grain rotation recrystallization can be excluded for the new grains because: (1) no progressive rota-



## Brittle-viscous deformation of vein quartz

H. J. Kjøll et al.

Title Page

Abstract

Introduction

Conclusions

References

Tables

Figures

⏪

⏩

◀

▶

Back

Close

Full Screen / Esc

Printer-friendly Version

Interactive Discussion



foliation through the growth of fine grained white mica at the expense of feldspar, transforming the host rock into a weak phyllonite and leading to strain partitioning (Tullis and Wenk, 1994). Syndeformational carbonation reactions have been proposed as a viable mechanism for the transformation of the originally massive Nussir basalts into foliated, weak phyllonites (Torgersen and Viola, 2014). Progressive metabasalt phyllonitization localized strain efficiently within the NFZ due to the reduction of internal friction and grain size reduction as the rock could deform more readily by grain boundary sliding and dissolution creep (e.g. Torgersen and Viola, 2014; Stünitz and Fitz Gerald, 1993). Within such a structural framework, plagioclase and quartz represented relatively competent porphyroclasts, deforming predominantly by granular flow (Fig. 4a). The studied quartz vein remained mostly unaffected by the phyllonitization, thus becoming a rigid object that escaped most deformation (Bell, 1985; Menegon et al., 2008; Tullis and Wenk, 1994), although some dissolution at the vein-matrix contact may have occurred (e.g. white arrows in Fig. 3b). The progressively increasing competence contrast between the phyllonitic matrix and the quartz vein generated significant strain partitioning, wherein coaxial deformation was accommodated by the quartz vein (e.g. the described conjugate shear bands) and non-coaxial deformation by the matrix, as shown by, for example, rotated porphyroclasts and asymmetric shear bands (e.g. Goodwin and Tikoff, 2002; Menegon et al., 2008). This rheological contrast is also believed to be crucial for the transient embrittlement of the quartz vein already argued for in the discussion above. Both the phyllonite  $S$  and  $C'$  planes, due to their interconnected anastomosed geometry and low coefficient of friction, deformed at a significantly higher strain rate than the quartz vein. This contrast enhanced dislocation tangling within the vein because deformation mechanisms within the matrix (such as dissolution and grain boundary sliding) were much more effective than glide-accommodated dislocation creep.

The NFZ deformed in a fluid rich system as shown by a plethora of microstructures within both the matrix and the vein quartz (e.g. Fig. 4). Several authors have stressed the importance of fluids in promoting viscous deformation in quartz (e.g. Kronenberg and Tullis, 1984; Mancktelow and Pennacchioni, 2004) and the role played by fracturing

in distributing fluids within a rigid body located in a weak matrix (Menegon et al., 2008). Calcite veinlets within the  $C'$  shear bands indicate multiple opening events and thus point towards a fluid pressure cyclicity ( $\lambda/\Delta\sigma$  plot in Fig. 10b–d). Similar conditions are also described from other parts of the PIS, such as the Kvenklubben fault some kilometers west of the NFZ (Torgersen and Viola, 2014).

Although the weak phyllonitic core of the NFZ could suggest that the fault deformed mainly by aseismic creep, the current fault architecture has to be projected against its temporal dynamic evolution. Initial strain accommodation occurred in fact under different rheological conditions, with transient embrittlement episodes and a possible seismic stick-slip behavior as also suggested from other localities within the PIS. Comparison of the microstructures described here with the results of Trepmann et al. (2007) thus corroborates the interpretation of the NFZ as a fault accommodating coseismic deformation.

The PIS has an overall geometry consistent with a Mohr–Coulomb mechanical wedge (Buitier, 2012) and is not significantly misoriented. The SFZ at the front of the imbricate, however, is highly misoriented, with an almost vertical dip (Fig. 1e). In addition, when moving, from the internal PIS in the NW toward the front of the stack, deformation becomes less penetrative, with local discrete faults developed on the limbs of progressively tightened folds (Torgersen and Viola, 2014). The cyclic fluid overpressuring as observed in the NFZ might have played an important role in steering deformation towards a more discrete accommodation style, resulting in cyclic oscillations between frictional and viscous deformation in a fault-valve behavior that facilitated the translation of the KNC to the foreland (Viola et al., 2006), but also possibly promoted seismic activity by stick-slip behavior. The SFZ misorientation can also be readily interpreted in such a scenario.

## SED

7, 213–257, 2015

### Brittle-viscous deformation of vein quartz

H. J. Kjølil et al.

Title Page

Abstract

Introduction

Conclusions

References

Tables

Figures



Back

Close

Full Screen / Esc

Printer-friendly Version

Interactive Discussion



## 6 Conclusion

The microstructures presented in this study contribute to the refined understanding of the mechanisms that accommodate strain in quartz during deformation at the brittle–viscous transition. Our observations confirm results from earlier studies and in addition allow refining existing conceptual models by showing that:

1. Under fluid-rich conditions typical of lower greenschist facies metamorphism, quartz may fracture pervasively along several intracrystalline planes such as the prism and basal plane, in addition to the rhomb. The exploited direction of preferential fracturing depends upon its orientation with respect to the imposed stress field.
2. Viscous weakening mechanisms, such as effective crystal plastic deformation, may reduce the need for embrittlement. However, if crystals are misoriented for optimal dislocation glide, strain hardening occurs, which promotes the onset of frictional deformation. Microfracturing and viscous deformation may, however, occur broadly coevally.
3. Nucleation processes can heal and seal the microfractures. Solution-precipitation is the mechanism believed to control the process. No recovery by sub grain rotation recrystallization is observed.
4. Cyclic fluid pressure oscillations promoted continuous switches in deformation mechanisms that resulted in transient and possibly seismogenic frictional deformation processes, These were rapidly followed by aseismic creep as fluids were vented and the host phyllonite developed a penetrative, thoroughgoing anastomosing network of weak slip planes.
5. Fluid assisted break-down of the host metabasalt formed the weak phyllonite, which promoted strain partitioning into the matrix rather than in the quartz vein, which escaped most strain. Rheological contrasts between the weak, foliated host

### Brittle-viscous deformation of vein quartz

H. J. Kjøll et al.

Title Page

Abstract

Introduction

Conclusions

References

Tables

Figures



Back

Close

Full Screen / Esc

Printer-friendly Version

Interactive Discussion



and the more rigid quartz vein also contributed to the transient embrittlement of quartz in the vein, providing positive feedback to the embrittlement caused by the presence of overpressured fluids.

*Acknowledgements.* The Geological Survey of Norway and the Norwegian University of Science and Technology have supported the preparation of this manuscript financially. Thank you Espen Torgersen for all the long and fruitful discussions and hours in front of the microscope, it is greatly appreciated!

## References

- Adams, B. L., Wright, S. I., and Kunze, K.: Orientation imaging: the emergence of a new microscopy, *Metall. Trans. A*, 24, 819–831, 1993.
- Atkinson, B. K.: Subcritical crack propagation in rocks: theory, experimental results and applications, *J. Struct. Geol.*, 4, 41–56, 1982.
- Atkinson, B. K.: Subcritical crack growth in geological materials, *J. Geophys. Res.-Sol. Ea.*, 89, 4077–4114, 1984.
- Bachmann, F., Hielscher, R., and Schaeben, H.: Texture analysis with MTEX–free and open source software toolbox, *Sol. St. Phen.*, 160, 63–68, 2010.
- Bell, T.: Deformation partitioning and porphyroblast rotation in meta-morphic rocks: a radical reinterpretation, *J. Metamorph. Geol.*, 3, 109–118, 1985.
- Bestmann, M. and Prior, D. J.: Intragranular dynamic recrystallization in naturally deformed calcite marble: diffusion accommodated grain boundary sliding as a result of subgrain rotation recrystallization, *J. Struct. Geol.*, 25, 1597–1613, 2003.
- Buiter, S. J.: A review of brittle compressional wedge models, *Tectonophysics*, 530, 1–17, 2012.
- Chen, Y., Hjelen, J., Gireesh, S., and Roven, H.: Optimization of EBSD parameters for ultra-fast characterization, *J. Microsc.-Oxford*, 245, 111–118, 2012.
- Cox, S. F.: The application of failure mode diagrams for exploring the roles of fluid pressure and stress states in controlling styles of fracture-controlled permeability enhancement in faults and shear zones, *Geofluids*, 10, 217–233, 2010.
- Dallmeyer, R. D., Mitchell, J. G., Pharaoh, T. C., Reuter, A., and Andresen, A.: K–Ar and Ar-40/Ar-39 whole-rock ages of slate phyllite from allochthonous basement and cover in

## Brittle-viscous deformation of vein quartz

H. J. Kjøl et al.

Title Page

Abstract

Introduction

Conclusions

References

Tables

Figures



Back

Close

Full Screen / Esc

Printer-friendly Version

Interactive Discussion



## Brittle-viscous deformation of vein quartz

H. J. Kjøl et al.

Title Page

Abstract

Introduction

Conclusions

References

Tables

Figures



Back

Close

Full Screen / Esc

Printer-friendly Version

Interactive Discussion



the tectonic windows of Finnmark, Norway – evaluating the extent and timing of caledonian tectonothermal activity, *Geol. Soc. Am. Bull.*, 100, 1493–1501, doi:10.1130/0016-7606(1988)100<1493:Kaaaaw>2.3.Co;2, 1988.

Dell'Angelo, L. N. and Tullis, J.: Textural and mechanical evolution with progressive strain in experimentally deformed aplite, *Tectonophysics*, 256, 57–82, 1996.

den Brok, S. W. J.: An Experimental Investigation into the Effect of Water on the Flow of Quartzite, Utrecht University, Holland, 1992.

den Brok, S. and Spiers, C.: Experimental evidence for water weakening of quartzite by micro-cracking plus solution-precipitation creep, *J. Geol. Soc. London*, 148, 541–548, 1991.

Derez, T., Pennock, G., Drury, M., and Sintubin, M.: Low-temperature intracrystalline deformation microstructures in quartz, *J. Struct. Geol.*, doi:10.1016/j.jsg.2014.07.015, online first, 2014.

Drury, M. R. and Urai, J. L.: Deformation-related recrystallization processes, *Tectonophysics*, 172, 235–253, 1990.

Fairbairn, H.: Correlation of quartz deformation with its crystal structure, *Am. Mineral.*, 24, 351–368, 1939.

Flörke, O. W., Mielke, H. G., Weichert, J., and Kulke, H.: Quartz with rhombohedral cleavage from Madagascar, *Am. Mineral.*, 66, 596–600, 1981.

Fron del, C., Dana, J. D., and Dana, E. S.: *The System of Mineralogy: Silica Minerals*, Wiley, New York, 1962.

Gee, D. G., Fossen, H., Henriksen, N., and Higgins, A. K.: From the early Paleozoic platforms of Baltica and Laurentia to the Caledonide Orogen of Scandinavia and Greenland, *Episodes*, 31, 44–51, 2008.

Goodwin, L. B. and Tikoff, B.: Competency contrast, kinematics, and the development of foliations and lineations in the crust, *J. Struct. Geol.*, 24, 1065–1085, 2002.

Hippertt, J. and Egydio-Silva, M.: New polygonal grains formed by dissolution–re-deposition in quartz mylonite, *J. Struct. Geol.*, 18, 1345–1352, 1996.

Hirth, G. and Tullis, J.: Dislocation creep regimes in quartz aggregates, *J. Struct. Geol.*, 14, 145–159, doi:10.1016/0191-8141(92)90053-Y, 1992.

Holyoke, C. W. and Tullis, J.: Mechanisms of weak phase interconnection and the effects of phase strength contrast on fabric development, *J. Struct. Geol.*, 28, 621–640, 2006.

## Brittle-viscous deformation of vein quartz

H. J. Kjøl et al.

Title Page

Abstract

Introduction

Conclusions

References

Tables

Figures



Back

Close

Full Screen / Esc

Printer-friendly Version

Interactive Discussion



- Hubbert, M. K. and Rubey, W. W.: Role of fluid pressure in mechanics of overthrust faulting, I. Mechanics of fluid-filled porous solids and its application to overthrust faulting, *Geol. Soc. Am. Bull.*, 70, 115–166, 1959.
- Kronenberg, A. K. and Tullis, J.: Flow strengths of quartz aggregates: grain size and pressure effects due to hydrolytic weakening, *J. Geophys. Res.-Sol. Ea.*, 89, 4281–4297, 1984.
- Kronenberg, A. K., Segall, P., and Wolf, G. H.: Hydrolytic weakening and penetrative deformation within a natural shear zone, in: *The Brittle–Ductile Transition in Rocks*, American Geophysical Union, Washington, D.C., 21–36, 1990.
- Mainprice, D., Hielscher, R., and Schaeben, H.: Calculating anisotropic physical properties from texture data using the MTEX open-source package, *Geol. Soc. Spec. Publ.*, 360, 175–192, 2011.
- Mancktelow, N. S. and Pennacchioni, G.: The influence of grain boundary fluids on the microstructure of quartz-feldspar mylonites, *J. Struct. Geol.*, 26, 47–69, 2004.
- Menegon, L., Pennacchioni, G., Heilbronner, R., and Pittarello, L.: Evolution of quartz microstructure and *c*-axis crystallographic preferred orientation within ductilely deformed granitoids (Arolla unit, Western Alps), *J. Struct. Geol.*, 30, 1332–1347, doi:10.1016/j.jsg.2008.07.007, 2008.
- Moen, K., Hjelen, J., and Malvik, T.: Preparation of Quartz samples for EBSD analysis, poster presented at the Applied Mineralogy '03 Conference, Helsinki, 17–18 March 2003.
- Pharaoh, T., Macintyre, R., and Ramsay, D.: K–Ar age determinations on the Raipas suite in the Komagfjord Window, Northern Norway, *Norsk Geol. Tidsskr.*, 62, 51–57, 1982.
- Pharaoh, T. C., Ramsay, D. M., and Jansen, Ø.: Stratigraphy and structure of the northern part of the Repparfjord-Komagfjord Window, Finnmark, Northern Norway, *Norg. Geol. Unders. B.*, 337, 1–45, 1983.
- Platt, J. and Vissers, R.: Extensional structures in anisotropic rocks, *J. Struct. Geol.*, 2, 397–410, 1980.
- Prior, D. J., Boyle, A. P., Brenker, F., Cheadle, M. C., Day, A., Lopez, G., Peruzzo, L., Potts, G. J., Reddy, S., and Spiess, R.: The application of electron backscatter diffraction and orientation contrast imaging in the SEM to textural problems in rocks, *Am. Mineral.*, 84, 1741–1759, 1999.
- Prior, D. J., Mariani, E., and Wheeler, J.: EBSD in the earth sciences: applications, common practice, and challenges, in: *Electron Backscatter Diffraction in Materials Science*, Springer US, 345–360, doi:10.1007/978-0-387-88136-2\_26, 2009.

## Brittle-viscous deformation of vein quartz

H. J. Kjøll et al.

Title Page

Abstract

Introduction

Conclusions

References

Tables

Figures



Back

Close

Full Screen / Esc

Printer-friendly Version

Interactive Discussion



Rice, A. H. N.: Stretching lineations and structural evolution of the Kalak Nappe Complex (Middle Allochthon) in the Repparfjord–Faegfjord area, Finnmark, northern Norway, *Norsk Geol. Tidsskr.*, 78, 277–289, 1998.

Roberts, D.: The Scandinavian Caledonides: event chronology, paleogeographic settings and likely modern analogues, *Tectonophysics*, 365, 283–299, doi:10.1016/S0040-1951(03)00026-X, 2003.

Schmid, S. and Casey, M.: Complete fabric analysis of some commonly observed quartz *c*-axis patterns, in: *Mineral and Rock Deformation: Laboratory Studies: The Paterson Volume*, American Geophysical Union, Washington, D.C., 263–286, doi:10.1029/GM036p0263, 1986.

Schneider, C. A., Rasband, W. S., Eliceiri, K. W., Schindelin, J., Arganda-Carreras, I., Frise, E., Kaynig, V., Longair, M., Pietzsch, T., and Preibisch, S.: 671 nih image to imageJ: 25 years of image analysis, *Nat. Methods*, 9, 671–675, doi:10.1038/nmeth.2089, 2012.

Segall, P. and Simpson, C.: Nucleation of ductile shear zones on dilatant fractures, *Geology*, 14, 56–59, 1986.

Stipp, M. and Kunze, K.: Dynamic recrystallization near the brittle–plastic transition in naturally and experimentally deformed quartz aggregates, *Tectonophysics*, 448, 77–97, 2008.

Stipp, M., Stunitz, H., Heilbronner, R., and Schmid, S. M.: The eastern Tonale fault zone: a “natural laboratory” for crystal plastic deformation of quartz over a temperature range from 250 to 700 degrees C, *J. Struct. Geol.*, 24, 1861–1884, doi:10.1016/S0191-8141(02)00035-4, 2002.

Stünitz, H. and Fitz Gerald, J.: Deformation of granitoids at low metamorphic grade. II: Granular flow in albite-rich mylonites, *Tectonophysics*, 221, 299–324, 1993.

Torgersen, E. and Viola, G.: Structural and temporal evolution of a reactivated brittle–ductile fault – Part I: Fault architecture, strain localization mechanisms and deformation history, *Earth Planet. Sc. Lett.*, 407, 205–220, doi:10.1016/j.epsl.2014.09.019, 2014.

Torgersen, E., Viola, G., Zwingmann, H., and Harris, C.: Structural and temporal evolution of a reactivated brittle–ductile fault – Part II: Timing of fault initiation and reactivation by K–Ar dating of synkinematic illite/muscovite, *Earth Planet. Sc. Lett.*, 407, 221–233, 2014.

Trepmann, C. A., Stöckhert, B., Dorner, D., Moghadam, R. H., Küster, M., and Röller, K.: Simulating coseismic deformation of quartz in the middle crust and fabric evolution during post-seismic stress relaxation – an experimental study, *Tectonophysics*, 442, 83–104, 2007.

## Brittle-viscous deformation of vein quartz

H. J. Kjøll et al.

Title Page

Abstract

Introduction

Conclusions

References

Tables

Figures

⏪

⏩

◀

▶

Back

Close

Full Screen / Esc

Printer-friendly Version

Interactive Discussion



Trepmann, C. A. and Stöckhert, B.: Microfabric of folded quartz veins in metagreywackes: dislocation creep and subgrain rotation at high stress, *J. Metamorph. Geol.*, 27, 555–570, doi:10.1111/j.1525-1314.2009.00842.x, 2009.

5 Tullis, J. and Wenk, H.-R.: Effect of muscovite on the strength and lattice preferred orientations of experimentally deformed quartz aggregates, *Mat. Sc.d Eng. A-Struct.*, 175, 209–220, 1994.

van Daalen, M., Heilbronner, R., and Kunze, K.: Orientation analysis of localized shear deformation in quartz fibres at the brittle–ductile transition, *Tectonophysics*, 303, 83–107, doi:10.1016/s0040-1951(98)00264-9, 1999.

10 Vernooij, M. G., den Brok, B., and Kunze, K.: Development of crystallographic preferred orientations by nucleation and growth of new grains in experimentally deformed quartz single crystals, *Tectonophysics*, 427, 35–53, 2006a.

Vernooij, M. G., Kunze, K., and den Brok, B.: “Brittle”shear zones in experimentally deformed quartz single crystals, *J. Struct. Geol.*, 28, 1292–1306, 2006b.

15 Viola, G., Mancktelow, N. S., and Miller, J. A.: Cyclic frictional–viscous slip oscillations along the base of an advancing nappe complex: insights into brittle-ductile nappe emplacement mechanisms from the Naukluft Nappe Complex, central Namibia, *Tectonics*, 25, TC3016, doi:10.1029/2005tc001939, 2006.

20 Vollbrecht, A., Stipp, M., and Olesen, N. Ø.: Crystallographic orientation of microcracks in quartz and inferred deformation processes: a study on gneisses from the German Continental Deep Drilling Project (KTB), *Tectonophysics*, 303, 279–297, 1999.

## Brittle-viscous deformation of vein quartz

H. J. Kjølil et al.

Title Page

Abstract

Introduction

Conclusions

References

Tables

Figures



Back

Close

Full Screen / Esc

Printer-friendly Version

Interactive Discussion



**Table 1.** Summary of microstructures.

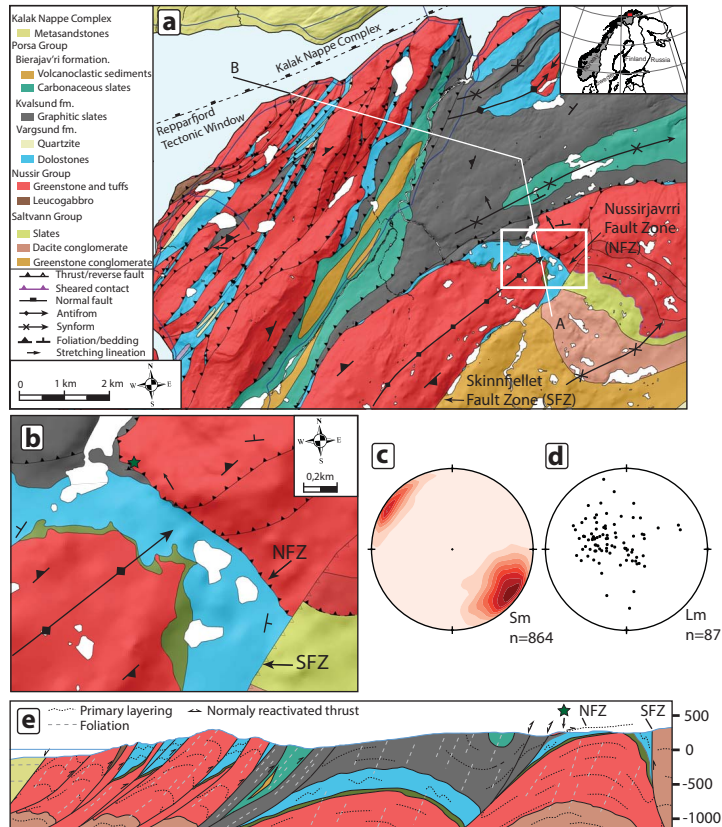
Domain	Old grain orientation	Microstructure type	Orientation of bands of new nucleated grains	Orientation of bands of new nucleated grains	Average grain size ( $\mu\text{m}$ )	Average aspect ratio
1	<C> 	Pervasive nucleation; “striped tiger” pattern	to $\{m\}$ and    to $\{r\}$	ca. $23^\circ$ and ca. $138^\circ$	Avg.: 15.51 Max.: 52.46 Min.: 4.47	1.63
2	<C> 	Dominated by new nucleated grains	to basal plane	ca. $160^\circ$	Avg.: 18.03 Max.: 55.32 Min.: 4.26	1.66
3	<C> 	Limited nucleation along a few bands	to basal plane and    to $\{r\}$	ca. $20^\circ$ and ca. $150^\circ$	Avg.: 13.96 Max.: 32.76 Min.: 5.09	1.59
4	<C> 	localized nucleation; minor “striped tiger” pattern and pockets of new grains	to $\{m\}$ and    to $\{r\}$	ca. $120^\circ$ and ca. $50^\circ$	Avg.: 15.48 Max.: 41.16 Min.: 4.26	1.60

## SED

7, 213–257, 2015

Brittle-viscous  
deformation of vein  
quartz

H. J. Kjøll et al.



Title Page

Abstract

Introduction

Conclusions

References

Tables

Figures

◀

▶

◀

▶

Back

Close

Full Screen / Esc

Printer-friendly Version

Interactive Discussion



**Figure 1. (a)** 1 : 50 000 lithological and structural map of the northwestern part of the Repparfjord Tectonic Window. Doglegged line: trace of cross section in **(e)**. White rectangle: location of detailed map in **(b)** inset shows the location of the study area in northern Norway. **(b)** Close-up of NFZ and sample location. Green star indicates sample location. **(c, d)** Contoured foliation and stretching lineation measurements, respectively, from the mapped area (lower hemisphere projection). **(e)** Cross section along the doglegged line in **(a)**. Black dashed line: folded primary layering, grey dashed line: axial planar foliation. Green star: sample location.

## SED

7, 213–257, 2015

### Brittle-viscous deformation of vein quartz

H. J. Kjøl et al.

Title Page

Abstract

Introduction

Conclusions

References

Tables

Figures

⏪

⏩

◀

▶

Back

Close

Full Screen / Esc

Printer-friendly Version

Interactive Discussion



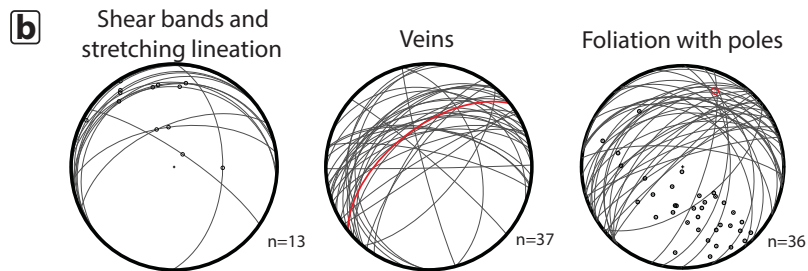


**Figure 2. (a)** Veins (outlined by black lines) cut by gently NNW-dipping shear bands (green dashed lines) that develop a pervasive EEC fabric at the outcrop scale. The NFZ fault core is located 2 m farther up. Sample location is indicated by the green star. Hammer handle for scale. **(b)** Orientation of key structural elements of the NFZ in lower hemisphere projections. Left stereonet: shear bands related to the NFZ and related stretching lineations. Middle stereonet: veins along the NFZ. The sampled vein is indicated by the red great circle. Right stereonet: great circles and poles of NFZ mylonitic and phyllonitic foliation planes indicating that the NFZ is folded around a calculated axis oriented 024/19 as indicated with a red point.

**Brittle-viscous deformation of vein quartz**

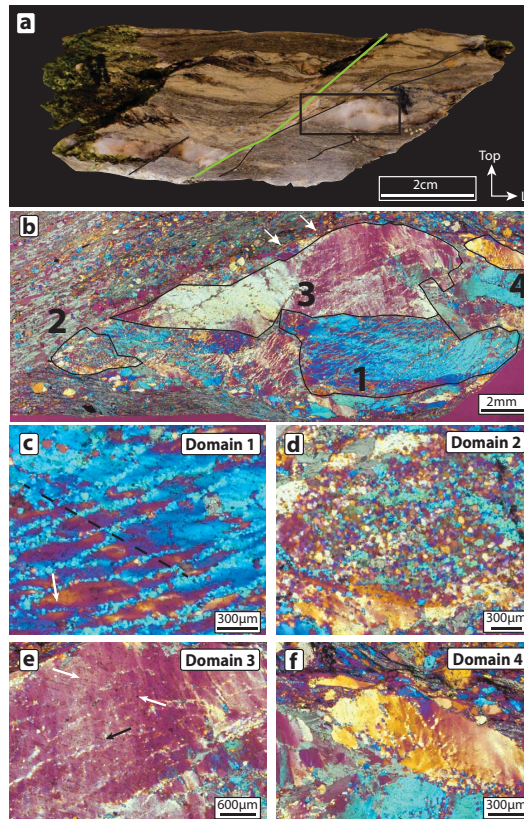
H. J. Kjølil et al.

Title Page	
Abstract	Introduction
Conclusions	References
Tables	Figures
◀	▶
◀	▶
Back	Close
Full Screen / Esc	
Printer-friendly Version	
Interactive Discussion	



**Brittle-viscous deformation of vein quartz**

H. J. Kjøl et al.



Title Page

Abstract

Introduction

Conclusions

References

Tables

Figures



Back

Close

Full Screen / Esc

Printer-friendly Version

Interactive Discussion



**Figure 3. (a)** Studied hand specimen. A discrete shear band (green line) cuts through the entire sample and offsets the studied quartz vein. Several second order shear bands (thick black lines) are also visible and some deform the vein with a smaller displacement. Black square: area of **(b)**. **(b)** Stitched overview microphotograph of the studied vein fragment. Black outlines outline distinct textural domains, labeled 1 through to 4. 2.5x, xpl and lambda plate inserted. **(c)** Close up of a representative area of *Domain 1*. Black dashed line: direction of wide extinction bands (WEB; Derez et al., 2014) seen as red-orange areas. White arrow: bridging band of new grains. 2.5x, xpl with lambda plate inserted. **(d)** Close up of representative microstructure of *Domain 2*. > 90% new grains. 2.5x, xpl and lambda plate inserted. **(e)** *Domain 3*. White arrows: trace of fluid inclusion plane. Black arrow: direction of band with new grains. 2.5x, xpl and lambda plate inserted. **(f)** Close up of *Domain 4* showing bands of new grains at a relatively high angle to each other. 2.5x, xpl and lambda plate inserted.

## SED

7, 213–257, 2015

### Brittle-viscous deformation of vein quartz

H. J. Kjølil et al.

Title Page

Abstract

Introduction

Conclusions

References

Tables

Figures

⏪

⏩

◀

▶

Back

Close

Full Screen / Esc

Printer-friendly Version

Interactive Discussion



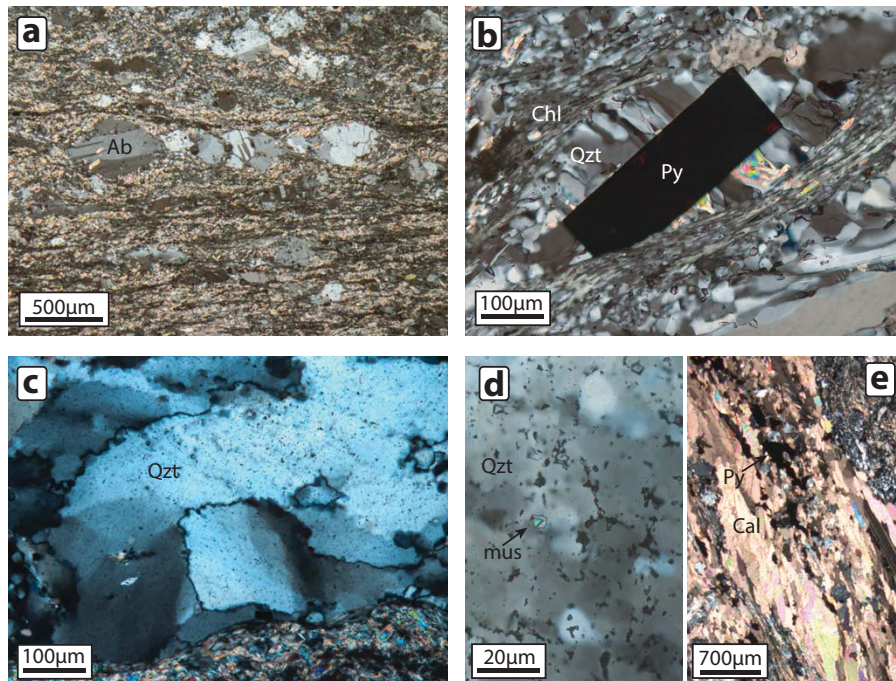


**Figure 4.** (a) Albite feldspar crystals asymmetrically cut and offset by dextral shear bands within the sheared, phyllosilicate-rich foliation of the NFZ. Minor recrystallization of the plagioclase can be seen in some of the shear bands. 5x, xpl. (b) Euhedral pyrite crystal partially altered to oxides (probably götite) with fibrous quartz and mica growing in the fringes, surrounded by chlorite. 20x, xpl. (c) Bulging grain boundaries and sub grains indicate low grade deformation of the vein quartz. 20x, xpl. (d) Small mica grain within a band of new grains in *Domain 2*. Large fluid inclusions outline the new grains and partially define the band. New grains are seen as different shades of grey. 40x, xpl. (e) Calcite veinlet displaying several opening events, with fine grained quartz at the matrix boundary with large, elongated calcite crystals and smaller equidimensional grains with some interspersed sulfides in the center. 2,5x, xpl.

**Brittle-viscous  
deformation of vein  
quartz**

H. J. Kjøll et al.

Title Page

Abstract

Introduction

Conclusions

References

Tables

Figures

◀

▶

◀

▶

Back

Close

Full Screen / Esc

Printer-friendly Version

Interactive Discussion



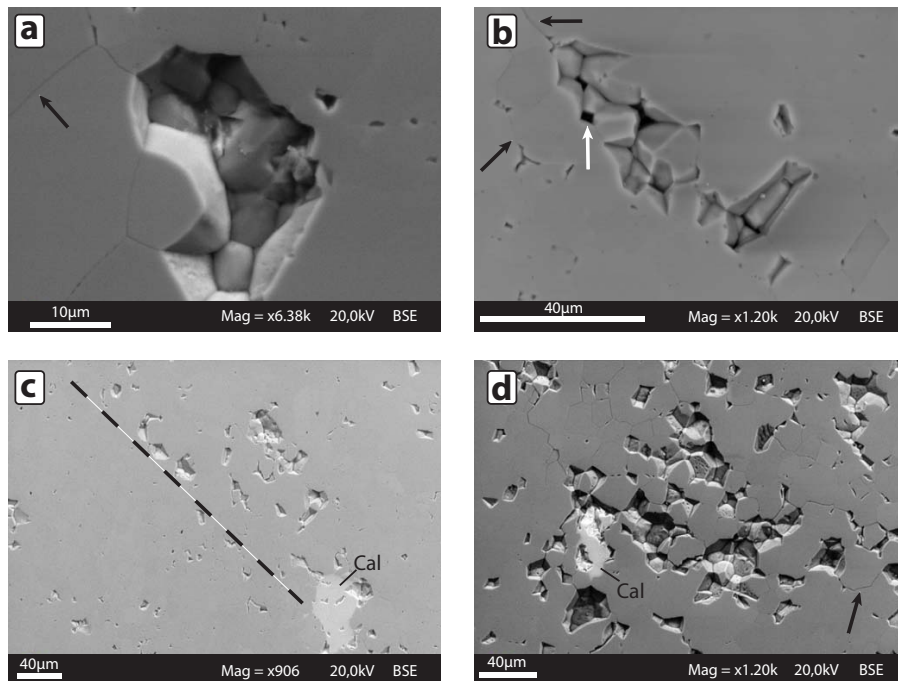


**Figure 5.** (a) Detailed BSE photograph of a pore between sub- to euhedral new grains. Sub-micron thick fractures between new grains as indicated by black arrow. (b) BSE image from *Domain 1*. Black areas as indicated by white arrow are holes. Black arrows indicate grain boundaries between new grains. New grains have a slight different shade of gray, due to a channeling effect. (c) BSE image from *Domain 1*. Fluid inclusions are spatially arranged in a pattern mimicking the orientation of a band (dashed line) of new grains. Secondary calcite is also present within the band, bounded by fluid inclusions. (d) BSE image from *Domain 2* showing a random distribution of fluid inclusions and narrow fractures encircling the new grains as indicated by black arrow.

**Brittle-viscous  
deformation of vein  
quartz**

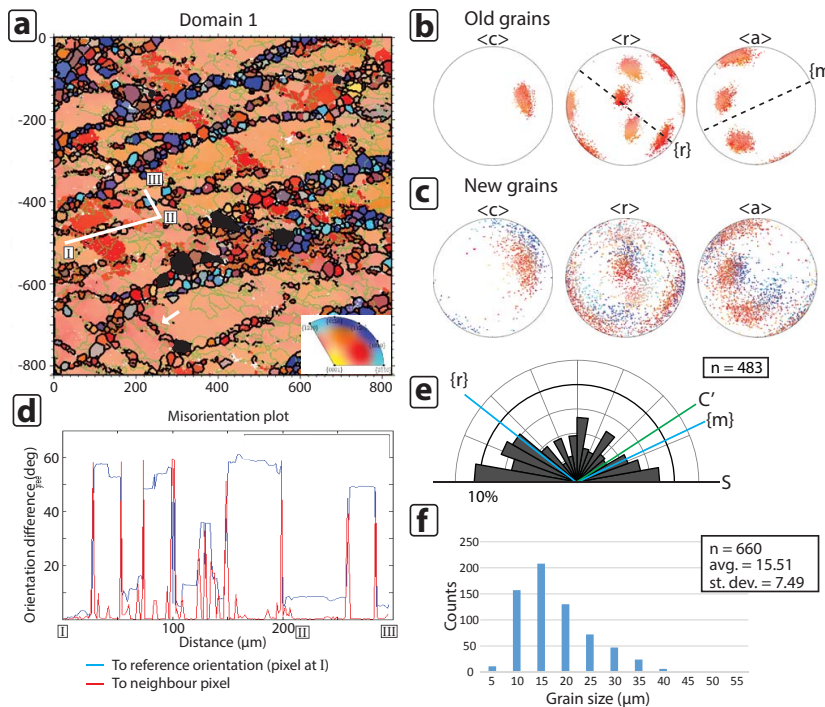
H. J. Kjøllet et al.

Title Page	
Abstract	Introduction
Conclusions	References
Tables	Figures
◀	▶
◀	▶
Back	Close
Full Screen / Esc	
Printer-friendly Version	
Interactive Discussion	



## Brittle-viscous deformation of vein quartz

H. J. Kjøllet et al.



Title Page

Abstract

Introduction

Conclusions

References

Tables

Figures



Back

Close

Full Screen / Esc

Printer-friendly Version

Interactive Discussion



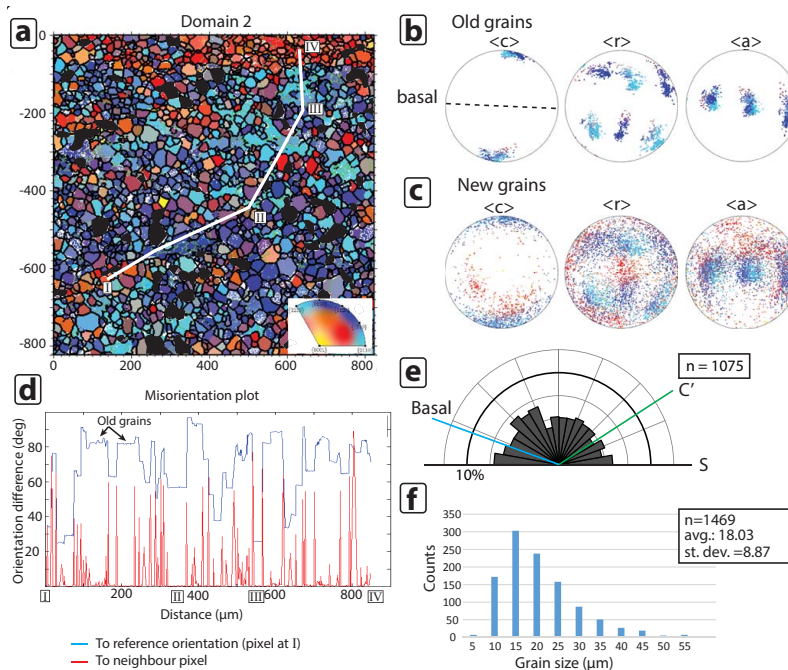


# SED

7, 213–257, 2015

## Brittle-viscous deformation of vein quartz

H. J. Kjøl et al.



Title Page

Abstract

Introduction

Conclusions

References

Tables

Figures



Back

Close

Full Screen / Esc

Printer-friendly Version

Interactive Discussion



**Figure 7.** Compilation of textural data from *Domain 2* (see Fig. 3b and d for its location). **(a)** EBSD map color coded according to color key in lower right corner of map. The map illustrates a section perpendicular to the foliation of the host rock and parallel to the stretching lineation. Black lines: grain boundaries defined by misorientations  $> 10^\circ$ . Green lines: sub grain boundaries defined by misorientations  $< 10^\circ$ . Black grains are calcite. White line I–IV: trace of misorientation profile in **(d)**. **(b, c)** Scatter orientation plots of  $\langle c \rangle$ ,  $\langle r \rangle$  and  $\langle a \rangle$  axis for old and new grains, respectively. The stereograms are upper hemisphere projections of 10 000 random points. Dashed lines represent trace of bands of new grains and which crystallographic plane it is parallel to. **(d)** Misorientation plot displaying difference in orientation to neighbor pixel (red line) and to reference orientation (i.e. orientation of pixel at A; blue line). **(e)** Rose diagram displaying the orientation of the long axis of the new grains with respect to the trace of  $C'$ ,  $S$  and the crystallographic planes which the bands are parallel to. **(f)** Histogram displaying grain size distribution of the new grains.

## SED

7, 213–257, 2015

### Brittle-viscous deformation of vein quartz

H. J. Kjølil et al.

Title Page

Abstract

Introduction

Conclusions

References

Tables

Figures

⏪

⏩

◀

▶

Back

Close

Full Screen / Esc

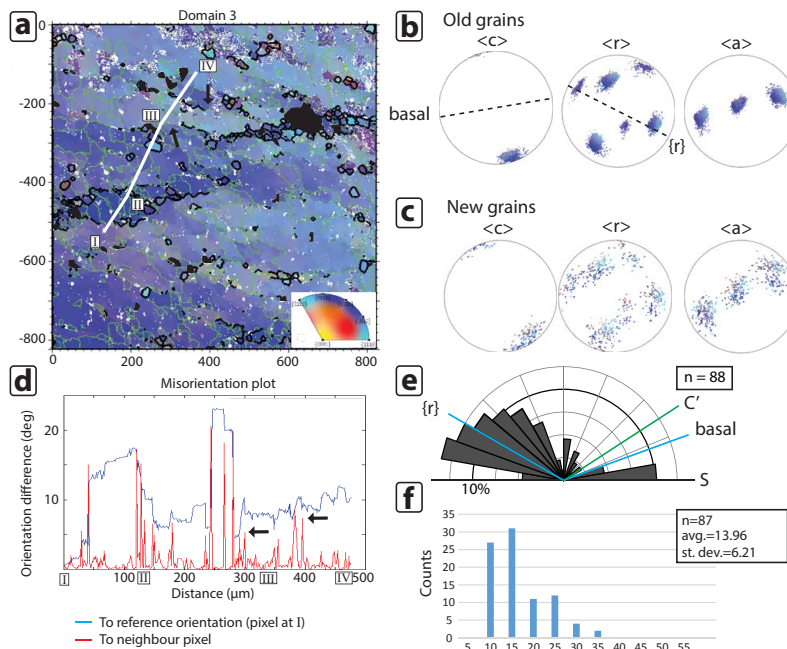
Printer-friendly Version

Interactive Discussion



## Brittle-viscous deformation of vein quartz

H. J. Kjøl et al.



Title Page

Abstract

Introduction

Conclusions

References

Tables

Figures



Back

Close

Full Screen / Esc

Printer-friendly Version

Interactive Discussion



**Figure 8.** Compilation of textural data from *Domain 3* (see Fig. 3b and e for its location). **(a)** EBSD map color coded according to color key in lower right corner of map. The map illustrates a section perpendicular to the foliation of the host rock and parallel to the stretching lineation. Black lines: grain boundaries defined by misorientations  $> 10^\circ$ . Green lines: sub grain boundaries defined by misorientations  $< 10^\circ$ . Black grains are calcite. White line I–IV: trace of misorientation profile in **(d)**. **(b, c)** Scatter orientation plots of  $\langle c \rangle$ ,  $\langle r \rangle$  and  $\langle a \rangle$  axis for old and new grains, respectively. The stereograms are upper hemisphere projections of 10 000 random points. Dashed lines represent trace of bands of new grains and which crystallographic plane it is parallel to. **(d)** Misorientation plot displaying difference in orientation to neighbor pixel (red line) and to reference orientation (i.e. orientation of pixel at A; blue line). **(e)** Rose diagram displaying the orientation of the long axis of the new grains with respect to the trace of  $C'$ ,  $S$  and the crystallographic planes which the bands are parallel to. **(f)** Histogram displaying grain size distribution of the new grains.

## SED

7, 213–257, 2015

### Brittle-viscous deformation of vein quartz

H. J. Kjølil et al.

Title Page

Abstract

Introduction

Conclusions

References

Tables

Figures

⏪

⏩

◀

▶

Back

Close

Full Screen / Esc

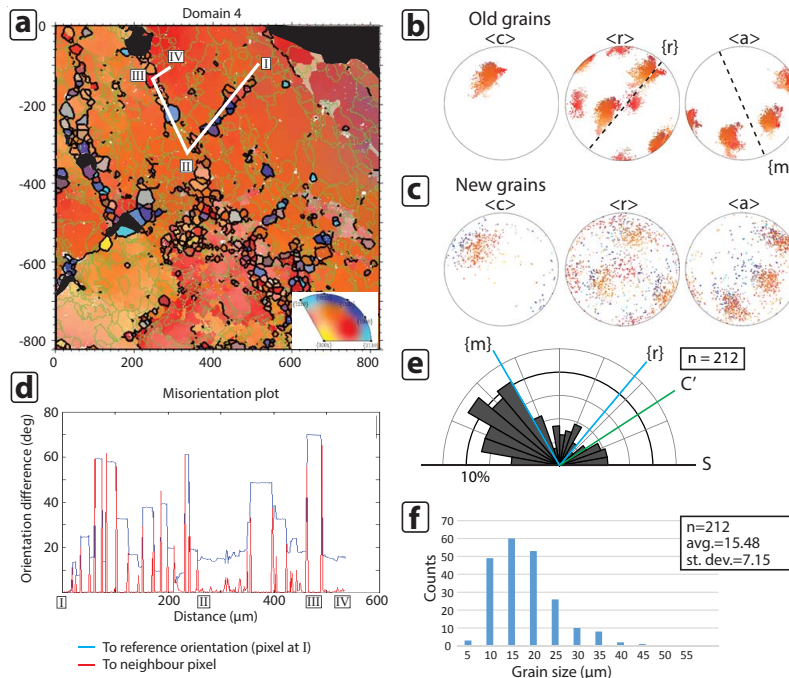
Printer-friendly Version

Interactive Discussion



## Brittle-viscous deformation of vein quartz

H. J. Kjøl et al.



Title Page

Abstract

Introduction

Conclusions

References

Tables

Figures



Back

Close

Full Screen / Esc

Printer-friendly Version

Interactive Discussion



**Figure 9.** Compilation of textural data from *Domain 4* (see Fig. 3b and f for its location). **(a)** EBSD map color coded according to color key in lower right corner of map. The map illustrates a section perpendicular to the foliation of the host rock and parallel to the stretching lineation. Black lines: grain boundaries defined by misorientations  $> 10^\circ$ . Green lines: sub grain boundaries defined by misorientations  $< 10^\circ$ . Black grains are calcite. White line I–IV: trace of misorientation profile in **(d)**. **(b, c)** Scatter orientation plots of  $\langle c \rangle$ ,  $\langle r \rangle$  and  $\langle a \rangle$  axis for old and new grains, respectively. The stereograms are upper hemisphere projections of 10 000 random points. Dashed lines represent trace of bands of new grains and which crystallographic plane it is parallel to. **(d)** Misorientation plot displaying difference in orientation to neighbor pixel (red line) and to reference orientation (i.e. orientation of pixel at A; blue line). **(e)** Rose diagram displaying the orientation of the long axis of the new grains with respect to the trace of  $C'$ ,  $S$  and the crystallographic planes which the bands are parallel to. **(f)** Histogram displaying grain size distribution of the new grains.

## SED

7, 213–257, 2015

### Brittle-viscous deformation of vein quartz

H. J. Kjøl et al.

Title Page

Abstract

Introduction

Conclusions

References

Tables

Figures

⏪

⏩

◀

▶

Back

Close

Full Screen / Esc

Printer-friendly Version

Interactive Discussion



## Brittle-viscous deformation of vein quartz

H. J. Kjølil et al.

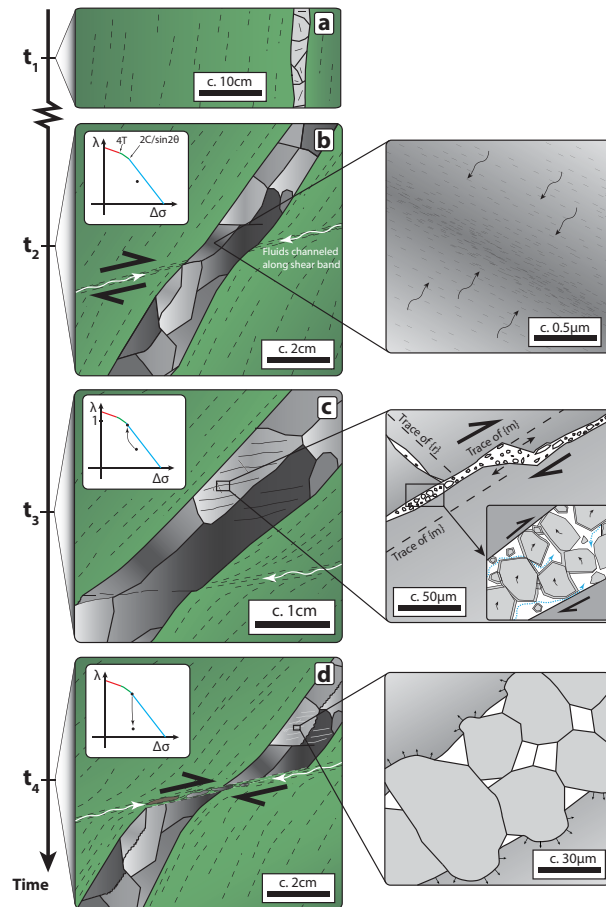


**Figure 10.** Conceptual sketch of the temporal evolution of the studied quartz vein with associated microstructures. See text for further details.  $\lambda$ - $\Delta\sigma$  diagrams (Cox, 2010) illustrate the transient evolution of fluid overpressure.

[Title Page](#)
[Abstract](#)
[Introduction](#)
[Conclusions](#)
[References](#)
[Tables](#)
[Figures](#)
[Back](#)
[Close](#)
[Full Screen / Esc](#)
[Printer-friendly Version](#)
[Interactive Discussion](#)